Estimating ROI activity concentration with photon-processing and photon-counting SPECT imaging systems

Abhinav K. Jha and Eric C. Frey

Division of Medical Imaging Physics, Department of Radiology, Johns Hopkins University, Baltimore, MD, USA

ABSTRACT

Recently a new class of imaging systems, referred to as photon-processing (PP) systems, are being developed that uses real-time maximum-likelihood (ML) methods to estimate multiple attributes per detected photon and store these attributes in a list format. PP systems could have a number of potential advantages compared to systems that bin photons based on attributes such as energy, projection angle, and position, referred to as photon-counting (PC) systems. For example, PP systems do not suffer from binning-related information loss and provide the potential to extract information from attributes such as energy deposited by the detected photon. To quantify the effects of this advantage on task performance, objective evaluation studies are required. We performed this study in the context of quantitative 2-dimensional single-photon emission computed tomography (SPECT) imaging with the end task of estimating the mean activity concentration within a region of interest (ROI). We first theoretically outline the effect of null space on estimating the mean activity concentration, and argue that due to this effect, PP systems could have better estimation performance compared to PC systems with noise-free data. To evaluate the performance of PP and PC systems with noisy data, we developed a singular value decomposition (SVD)-based analytic method to estimate the activity concentration from PP systems. Using simulations, we studied the accuracy and precision of this technique in estimating the activity concentration. We used this framework to objectively compare PP and PC systems on the activity concentration estimation task. We investigated the effects of varying the size of the ROI and varying the number of bins for the attribute corresponding to the angular orientation of the detector in a continuously rotating SPECT system. The results indicate that in several cases, PP systems offer improved estimation performance compared to PC systems.

Keywords: Photon-processing systems, Analytic ROI activity estimation, Null functions, Singular-value decomposition, SPECT, LM acquisition.

1. INTRODUCTION

In X-ray and gamma-ray imaging systems, the interaction of a photon with the detector can often be described using multiple parameters or attributes. For example, consider a single-photon emission computed tomography (SPECT) system consisting of modular scintillation cameras where each camera has a monolithic scintillator and an array of photo-multiplier tubes (PMTs). In this system, for each detected gamma-ray photon, we could use the PMT outputs to estimate the three-dimensional (3-D) coordinates of the position of interaction of the gamma-ray photon within the scintillator and the energy deposited at the interaction site. Similarly, we could also record the time of interaction and angular orientation of the detector when the interaction occurred. Further, we could estimate parameters related to secondary site interactions. Thus, for a SPECT system, we might have 8-10 attributes per detected photon. For a positron emission tomography (PET) system, the number of attributes could be almost double, as each coincidence event is detected by two scintillation cameras.

In conventional gamma-ray imaging systems, the attribute space is discretized into multiple bins, and the number of interaction events for which the attribute lies in the given bin are stored.[1] This leads to a binned image and is basically a histogram of the number of selected events for which the attribute lies within a certain range. The binned image is also referred to as the projection or sinogram image in nuclear imaging systems. We refer to systems that store data in this binned image format as photon-counting (PC) systems. This also includes systems that consist of pixellated detectors that output the number of photons that are incident on each pixel. The PC systems are described by a continuous-to-discrete (CD) operator.[1–6] In PC systems, the precise

Medical Imaging 2015: Physics of Medical Imaging, edited by Christoph Hoeschen, Despina Kontos,
Proc. of SPIE Vol. 9412, 94120R · © 2015 SPIE · CCC code: 1605-7422/15/$18 · doi: 10.1117/12.2082278

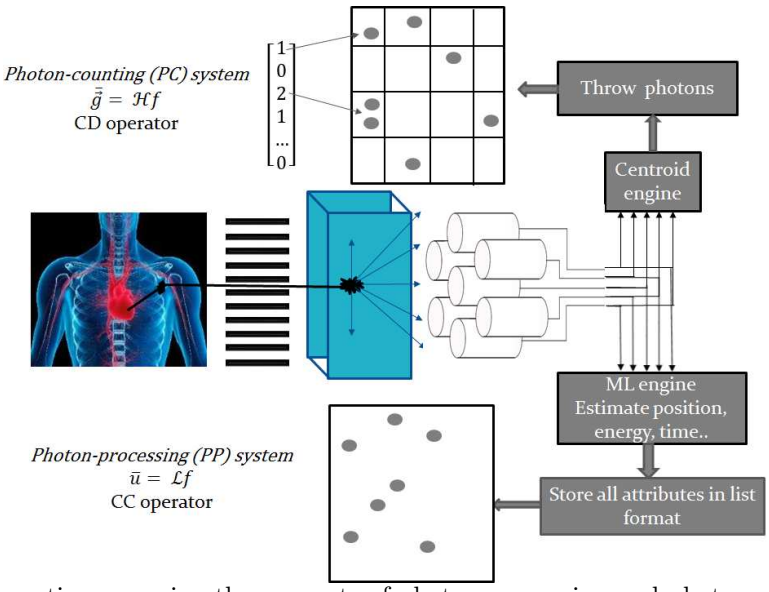

Figure 1: A schematic comparing the concepts of photon-processing and photon-counting systems

value of the attribute of each photon is lost due to the binning operation. For example, events with estimated energies of 126.3 and 140.5 keV would often be counted in the same, 126-154 keV energy window, leading to loss of information and two very different photons being treated the same way. Also, in PC systems, many photon attributes are ignored, since storing them in binned format generates high-dimensional images and it is impractical to process so many attributes. Moreover, many events are discarded, such as events where value of the energy attribute is outside the acquisition window or photons acquired during the time between projection views in step-and-shoot acquisition. Finally, the attributes are often estimated using a technique that might not be optimal, such as a centroid-based technique to estimate the position attributes.[1,7,8] All these processes result in loss of information.

To more completely use the information present in the detected photon, we could consider another class of systems where for each photon-interaction event, the measured sensor outputs are used to estimate the photon attributes using a real-time maximum-likelihood (ML) technique.[8,9] ML estimators have several properties that help in minimizing the information loss in the estimation process. ML estimators are efficient, i.e. they are unbiased and attain the Cramér-Rao lower bound (CRLB), if an efficient estimator exists. Further, the ML estimates are asymptotically efficient and consistent under most conditions[2] and these asymptotic properties of the ML estimates can be invoked in scintillation-detector based nuclear PP imaging systems.[8,10] Another important advantage of using ML estimation is that it yields an expression for the probability distribution function (PDF) of the estimated attributes. The estimated photon attributes are then stored at high precision in a list format, and we assume that this storage is almost full precision. With this assumption, the data are defined over a continuous domain and there is no binning-related information loss. We refer to the stored data as list-mode (LM) data, although it must be noted that our use of the term list-mode goes beyond conventional usage, primarily because of storing multiple photon attributes, the ML estimation of these attributes and their storage at high precision. Finally, we process the stored photon attributes on a per-photon basis. These systems are referred to as photon-processing (PP) systems.[6,11] The concept of photon-processing systems has its origins at the Center for Gamma Ray Imaging at the University of Arizona. Several such systems have been developed for nuclear imaging applications.[12–17] A schematic comparing the concepts of PP and PC systems is shown in Fig. 1.

PP systems have several advantages compared to PC systems, such as no binning-related information loss, a statistical model to account for the estimation-related information loss, and the possibility to use information from other attributes such as energy of the interaction event.[11,18] Our focus is to investigate any potential advantages gained due to the absence of binning-related information loss in PP systems. In a previous study, we made some

preliminary investigations of these advantages and our studies demonstrated that, in the absence of noise, for different phantoms, PP systems could potentially measure several object features that were not measured by PC systems.[11] However, it might be possible that the effects of noise could offset these advantages. To study the advantages of PP systems concretely in the effect of noise, objective evaluation studies are required. The objective evaluation studies are based on the underlying philosophy that medical images are acquired for a certain task, and thus imaging systems or algorithms should be evaluated based on their performance in the given task. The task of interest in this paper is estimating the mean activity concentration within a known region of interest (ROI) for quantitative 2-D SPECT imaging. This imaging task is important in several clinical applications such as targeted radionuclide therapy (TRT),[19–21] dopamine transporter scan (DaTSCAN) quantification,[22,23] and renal Tc-99m dimercaptosuccinic acid (DMSA) SPECT studies.[24,25]

To perform the objective evaluation study, we require a method to estimate the mean activity concentration from the PP systems. For this purpose, we have developed a singular-value decomposition (SVD)-based technique that can estimate the mean activity concentration directly from the photon attributes. The developed technique does not require the reconstruction of the object function. We use this technique in an objective evaluation study to compare the performance of PP and PC systems on the task of estimating activity concentration within a ROI.

The paper is organized in the following sections. In Sec. 2.1, we theoretically argue that in the absence of noise, PP systems could have improved estimation performance compared to PC systems. In Sec. 2.2, we derive the SVD-based analytical technique that determines the activity directly from the photon attributes. In Sec. 3, we describe the methods for the objective evaluation study. In Sec. 4, we study the performance of the algorithm on the activity estimation task for a continuously rotating PP SPECT system. We also objectively evaluate the performance of the PP and PC systems as the true activity concentration and ROI size are varied and analyze the effect of binning the attribute corresponding to angular orientation of the detector in the PC system. Finally, in Sec. 5, we summarize the important conclusions of the paper.

2. THEORY

2.1 Null functions and estimability

Consider a linear PC SPECT system, characterized by the system operator $\mathcal{H}$, imaging an object function $f(\boldsymbol{r})$, where $\boldsymbol{r}$ is a q-dimensional vector defined over $\mathbb{L}_2(\mathbb{R}^q)$. Let us define the ROI by a scaled support function $\chi(\boldsymbol{r})$. The ROI activity concentration that we intend to estimate is given by

$$\lambda = \int_{S_f} d^2 f(\boldsymbol{r})\chi(\boldsymbol{r}) = (\boldsymbol{\chi}, \boldsymbol{f}), \tag{1}$$

where $(\ldots,\ldots)$ denotes a scalar product of the quantity within the parentheses and S_f denotes the support of the object function. Further, in this manuscript, we will designate vectors by boldface type, so that $f(\boldsymbol{r})$ will be denoted by $\boldsymbol{f}$.

For a linear imaging system, we can define two orthogonal subspaces of the object space, termed as measurement and null space, such that

$$f(\boldsymbol{r}) = f_{\text{meas}}(\boldsymbol{r}) + f_{\text{null}}(\boldsymbol{r}), \tag{2}$$

and

$$\mathcal{H}\boldsymbol{f}_{\text{null}} = \boldsymbol{0}. \tag{3}$$

In other words, when the object is imaged through a linear imaging system, the null component of the object function $f_{\text{null}}(\boldsymbol{r})$ is not imaged, and cannot be retrieved even from the noise-free data. An object that consists of only these null components will be invisible to the imaging system and is termed as null function, invisible object, or ghost object of the imaging system.[26]

We can similarly decompose the ROI function for this imaging system as

$$\chi(\boldsymbol{r}) = \chi_{\text{meas}}(\boldsymbol{r}) + \chi_{\text{null}}(\boldsymbol{r}). \tag{4}$$

Substituting the expressions from Eqs. 2 and 4 in Eq. 1 and using the orthogonality of the measurement and null spaces yields[2]

$$\lambda = (\boldsymbol{\chi}_{\text{meas}}, \boldsymbol{f}_{\text{meas}}) + (\boldsymbol{\chi}_{\text{null}}, \boldsymbol{f}_{\text{null}}). \tag{5}$$

Since the imaging system is insensitive to $\boldsymbol{f}_{\text{null}}$ and $\boldsymbol{\chi}_{\text{null}}$, we can never recover the second term in Eq. 5 from even the noise-free image data. Thus, to obtain an accurate estimate of λ, this term should be as small as possible.

As described earlier, a PC system records the number of photon counts in a finite number of bins. Let us denote the number of bins by M, so that the acquired image, denoted by the vector $\boldsymbol{g}$, is an M-dimensional vector lying in the Euclidean vector space $\mathbb{E}^M$. Thus, the system maps from an infinite dimensional Hilbert space $\mathbb{L}_2(\mathbb{R}^q)$ to a finite-dimensional Eucledian space $\mathbb{E}^M$, and will have an infinite-dimensional null space due to dimensionality considerations.[11] Consequently, an infinite set of null functions exist for PC systems. On the contrary, a PP system acquires LM data that is defined over a continuous domain. If the PP system acquires s attributes per photon, then it can be shown that the PP system operator, denoted by $\mathcal{L}$, maps from the infinite-dimensional Hilbert space $\mathbb{L}_2(\mathbb{R}^q)$ to another infinite-dimensional Hilbert space $\mathbb{L}_2(\mathbb{R}^s)$. Thus, while the PP system might have a null space, if $s \geq q$, this null-space is not demanded by dimensionality considerations. Consequently, the various object and ROI functions would likely have a smaller null component for PP systems as compared to PC systems.

2.2 Algorithm to estimate activity concentration from PP systems

The analysis in the previous section indicates that due to null-space considerations, PP systems should estimate the activity concentration more accurately than PC systems for noise-free data. To quantify the improvement due to this advantage in terms of task performance, an objective evaluation study is required to evaluate the performance of PP and PC systems. To perform this study, we first derived a method to estimate the activity from the data acquired using PP systems.

The LM data acquired by a PP system is defined over a continuous domain. Thus, the PP imaging system can be described by a continuous-continuous (CC) system operator that relates the object function to the LM data.[27,28] We have used the CC nature of the PP imaging system operator to develop an SVD-based framework that estimates the continuous object function from LM data. We have used this framework to derive the reconstruction method for a continuously rotating hypothetical 2-D SPECT system with an ideal parallel-hole collimator.[11] Consider such a SPECT system that acquires LM data over π radians. The attributes acquired by this system are the position of interaction of the gamma-ray photon with the detector, denoted by $\hat{p}$, and the angular orientation of the detector, denoted by θ. Let us denote the number of events acquired by the PP system by J, where the j^{th} LM attribute vector consists of the estimated position of interaction with the detector, $\hat{p}_j$, and the angular orientation of the detector θ_j. The LM data acquired by this system can be described by the point process

$$u(\hat{p}, \theta) = \sum_{j=1}^{J} \delta(\hat{p} - \hat{p}_j)\delta(\theta - \theta_j). \tag{6}$$

For a given object $f(\boldsymbol{r})$, where $\boldsymbol{r}$ denotes a 2-D vector, and a fixed acquisition time τ, taking the mean of this point process over J and the photon attributes yields

$$\bar{u}(\hat{p}, \theta) = \tau \int_{\mathbb{S}_f} d^2r \text{pr}(\hat{p}, \theta|\boldsymbol{r}) s(\boldsymbol{r}) f(\boldsymbol{r}), \tag{7}$$

where $\text{pr}(\hat{p}, \theta|\boldsymbol{r})$ is the probability distribution function (PDF) for an event that originates with an emission at point $\boldsymbol{r}$, $s(\boldsymbol{r})$ is the probability that an event that originated at point $\boldsymbol{r}$ in the object space will be detected and included in the list of events, and $\mathbb{S}_f$ denotes the support of the functions in object space. Thus, the CC operator that describes this system has its kernel given by

$$l(\hat{p}, \theta, \boldsymbol{r}) = \tau \text{pr}(\hat{p}, \theta|\boldsymbol{r}) s(\boldsymbol{r}). \tag{8}$$

We have derived the SVD of this operator, and used the SVD to derive the pseudoinverse of the operator. Using the expression for the pseudoinverse, we were able to derive an expression to reconstruct the continuous object

function.[11] Let us denote the estimated activity distribution by the function $\hat{f}(\boldsymbol{r})$. Further, let us denote the variance of the estimation-related blur by σ_p. The expression that we have derived for the reconstructed object function with this PP system is given by[11,29]

$$\hat{f}(\boldsymbol{r}) = \frac{\pi}{\tau} \sum_{j=1}^{J} \mathcal{F}^{-1}\{|\rho| \exp(2\pi^2 \rho^2 \sigma^2)\}(\boldsymbol{r} \cdot \hat{\boldsymbol{n}}_{\theta_j} - \hat{p}_j), \tag{9}$$

where $\hat{\boldsymbol{n}}_{\theta_j}$ is the unit vector parallel to the detector, i.e. perpendicular to the projection direction, when the detector is aligned at an angle θ_j, ρ is the signed magnitude of the frequency vector $\boldsymbol{\rho}$, and $\mathcal{F}^{-1}$ denotes the inverse of the Fourier transform. Intuitively, this expression states that to reconstruct the object function, we must filter each LM event, shift the filtered output by a value equal to the position of interaction attribute of the LM event, and then backproject the result into object space at an angle given by the angular orientation attribute. To simplify the notation, we denote the filtering operation, i.e. the inverse Fourier transform in Eq. 9, by the expression $h(\boldsymbol{r} \cdot \hat{\boldsymbol{n}}_{\theta_j} - \hat{p}_j)$. With this notation, Eq. 9 can be rewritten as

$$\hat{f}(\boldsymbol{r}) = \frac{\pi}{\tau} \sum_{j=1}^{J} h(\boldsymbol{r} \cdot \hat{\boldsymbol{n}}_{\theta_j} - \hat{p}_j). \tag{10}$$

Denoting the ROI by $\chi(\boldsymbol{r})$, the estimate of the mean ROI activity concentration within this ROI, which we denote by $\hat{\lambda}$, is given by

$$\hat{\lambda} = \frac{1}{\int_{\mathbb{S}_f} d^2 r \chi(\boldsymbol{r})} \int_{\mathbb{S}_f} d^2 r \hat{f}(\boldsymbol{r}) \chi(\boldsymbol{r}). \tag{11}$$

Substituting the expression for $\hat{f}(\boldsymbol{r})$ from Eq. 9, we obtain

$$\hat{\lambda} = \frac{\pi}{A\tau} \sum_{j=1}^{J} \int_{\mathbb{S}_f} d^2 r h(\boldsymbol{r} \cdot \hat{\boldsymbol{n}}_{\theta_j} - \hat{p}_j) \chi(\vec{\boldsymbol{r}}), \tag{12}$$

where A denotes the area of the ROI. This expression computes the mean activity concentration by filtering and backprojecting all the LM events into object space and then integrating over the ROI. Replacing $\boldsymbol{r} \cdot \hat{\boldsymbol{n}}_{\theta_j} - \hat{p}_j$ by the variable q and using the sifting property of the delta functions, we can rewrite the above expression as

$$\hat{\lambda} = \frac{\pi}{A\tau} \sum_{j=1}^{J} \int_{\mathbb{S}_f} d^2 r \int_{\infty} dq h(q) \delta(q - \boldsymbol{r} \cdot \hat{\boldsymbol{n}}_{\theta_j} + \hat{p}_j) \chi(\boldsymbol{r}). \tag{13}$$

Changing the order of integration yields

$$\hat{\lambda} = \frac{\pi}{A\tau} \sum_{j=1}^{J} \int_{\infty} dq h(q) \int_{\mathbb{S}_f} d^2 r \delta(q - \boldsymbol{r} \cdot \hat{\boldsymbol{n}}_{\theta_j} + \hat{p}_j) \chi(\boldsymbol{r}). \tag{14}$$

In Eq. 14, the integral over $\boldsymbol{r}$ is the projection of the ROI on the detector. Thus, instead of backprojecting into the ROI and then convolving in the object space, we instead project the ROI in the detector space and then convolve with the filter function. This approach, which is similar to a previous approach for binned data[30] simplifies the computation, both analytically and numerically. Also, note that by exploiting the fact that the LM data is acquired over a continuous domain, and thus being able to derive an expression for the estimate of the continuous object function, we are able to estimate the activity without actually having to compute the object vector over a discrete grid. Thus, we avoid the reconstruction and discretization-related information loss.

An issue with this expression is that evaluating the inverse Fourier transform over an infinite interval is not possible since the integrand diverges even when we ignore the estimation-related blur. We found that the technique we used to evaluate the inverse Fourier transform for reconstructing the object function was not ideal

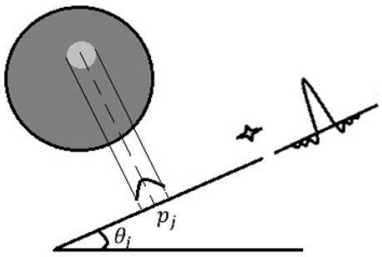

Figure 2: A schematic illustrating the computation of the activity in the projection space using the proposed algorithm

for absolute quantitation. We improved the method by instead evaluating the inverse Fourier transform, i.e. the expression $h(q)$, over a finite range. The approach is similar to a technique proposed in Ramachandran et al.[31] to reconstruct a three-dimensional object from its transmission shadowgraphs. We replace the limits $-\infty$ to ∞ by $-D/2$ to $D/2$, where D is some large finite number. In the limit of no estimation blur, we can thus define

$$h_D(q) = \int_{-D/2}^{D/2} d\rho |\rho| \exp(-2\pi i \rho q). \tag{15}$$

Ignoring the difference between $h_D(q)$ and $h(q)$ when D is large enough, we can evaluate this integral over a set of points na, where n is an integer and a is some small interval. The evaluation of the integral yields

$$h(na) = \begin{cases} \frac{1}{4a^2} \text{ for } n = 0. \\ \frac{-1}{\pi^2 n^2 a^2} \text{ for } n \text{ odd.} \\ 0 \text{ for } n \text{ even.} \end{cases} \tag{16}$$

We can substitute this expression in Eq. 14 and thus estimate the activity concentration in the absence of estimation-related blur. A schematic that illustrates the computation of the estimated activity in the projection space using the proposed algorithm is illustrated in Fig. 2.

We can also use Eq. 13 to derive the mean of the estimated ROI activity as below:

$$\bar{\hat{\lambda}} = \frac{1}{A} \int d\theta \int d^2\boldsymbol{r}' f(\boldsymbol{r}') \int dq h(q) \int d^2 r \delta(q - (\boldsymbol{r} - \boldsymbol{r}') \cdot \hat{\boldsymbol{n}}_{\theta_j}) \chi(\boldsymbol{r}). \tag{17}$$

3. METHODS

3.1 Imaging simulation

We modeled a hypothetical 2-D SPECT imaging system that rotated continuously. To generate the photon attributes for the PP system, we first determined the number of detected photons by sampling a Poisson distribution with a mean given by the total activity in the object. Since we ignored attenuation and scatter in this analysis, the probability of detection at each angle was constant. Thus, for the j^{th} LM event, the angular orientation of the detector θ_j was determined by sampling from a continuous uniform distribution of angle values between 0 and π radians. To determine the position of interaction p_j of this LM event, we used the Radon transform to analytically determine the projection data from the continuous object function at the projection angle θ_j. We treated this projection data as the probability density function (PDF) of p_j, and sampled this PDF to determine p_j. To perform this step numerically, the projection data were computed for finely spaced values of the position of interaction, yielding a binned representation of the the PDF of p_j, i.e. a histogram, of p_j. Then, using the inverse-transform sampling scheme,[32] we sampled this histogram to determine the bin to which p_j would belong. Uniformly sampling a location within this bin yielded p_j. Note that p_j was a continuous random variable, and not binned in any way, even though it was generated on a computer. To account for estimation blur, we then sampled another Gaussian distribution with mean equal to the true position of interaction, and variance equal to the variance of the estimation blur. We thus determined the estimated position of interaction $\hat{p}_j$

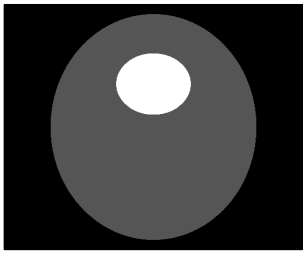

Figure 3: A representative object activity distribution for the objective evaluation study

for the LM event. However, in the experiments presented in this paper, the estimation-related blur was ignored. For each photon, the system recorded the position of interaction of the photon and the angular orientation of the detector. This yielded the PP system data that were stored in a list format.

To obtain the noisy PC system data, we binned the position attribute into 128 bins. Also, the angular orientation attribute was binned into a finite number of bins, the number of which was varied for different experiments.

3.2 Object model

The object had an elliptical support with uniform background activity over the support, and the ROI was a uniform-activity circular region within this support. A representative object activity distribution is shown in Fig. 3. The field of view was 40 cm, and the radius of the ROI was varied from 1 cm to 5 cm. We studied the performance of this algorithm at low counts using ROI activity concentrations from 120 Bq/cm^2 to 600 Bq/cm^2; the background activity was fixed to 100 Bq/cm^2. The detected counts varied from about $80,000$ to $170,000$ photons. With this object model and the imaging simulation procedure as described above, the experiment was repeated for forty noise realizations.

3.3 Estimating the activity concentration

We used Eq. 13 to estimate the activity concentration for the PP system. For the PC system, we used the filtered-back projection (FBP) algorithm to reconstruct the image over a 128×128 pixel grid. The FBP algorithm was chosen since it is often used for reconstructing object vectors with PC systems. Further, it is similar, and in many ways analogous to the SVD-based reconstruction approach for PP systems that was used to derive the analytic algorithm for estimating the activity concentration. For example, both the approaches are non-iterative and designed for 2-D SPECT systems with ideal parallel-hole collimators. The activity concentration within the ROI was subsequently estimated from this image.

4. RESULTS

The absolute value of the normalized bias and the standard deviation of the estimated activity concentration were computed and are plotted as a function of the mean activity concentration in Fig. 4 for two different ROI sizes for both PP and PC systems. It is observed that the PP system has a smaller bias and standard deviation as compared to PC system for all values of activity and both the ROI sizes. Also, the bias is much larger with PC system when the ROI radius was smaller. This is perhaps a consequence of the binning-related information loss being more pronounced when the ROI size is smaller.

In Fig. 5, the absolute value of the normalized bias and standard deviation of the estimated activity concentration are plotted as a function of the mean activity concentration for different numbers of projections. It is observed that the bias of the activity estimated from the PP system using our algorithm is lower than the bias for PC systems for even 128 projections. However, the standard deviation of the estimated activity is not consistently lower for PP systems in comparison to PC systems. This could be due to the finiteness in the number of LM events, and hints at a tradeoff between the information loss due to the effect of noise and binning the data. We are pursuing further studies in this direction.

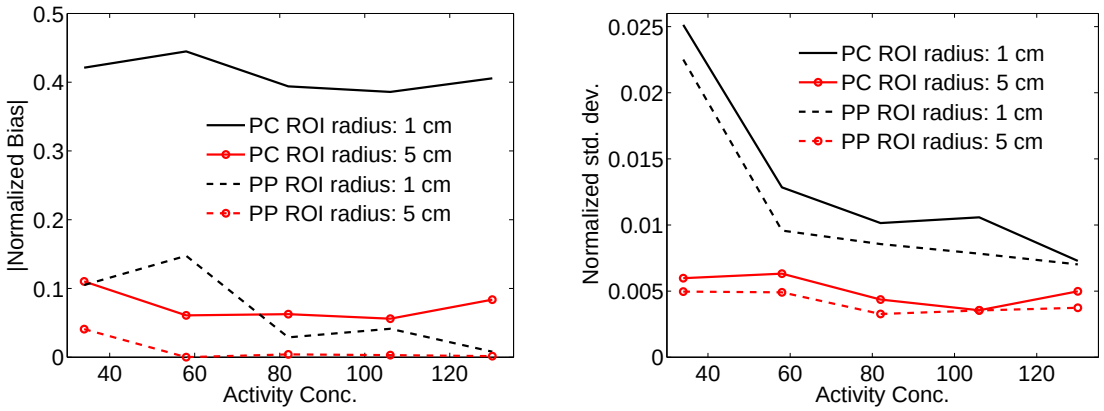

(a) (b)

Figure 4: (a) Normalized bias and (b) standard deviation of estimated activity for different ROI sizes.

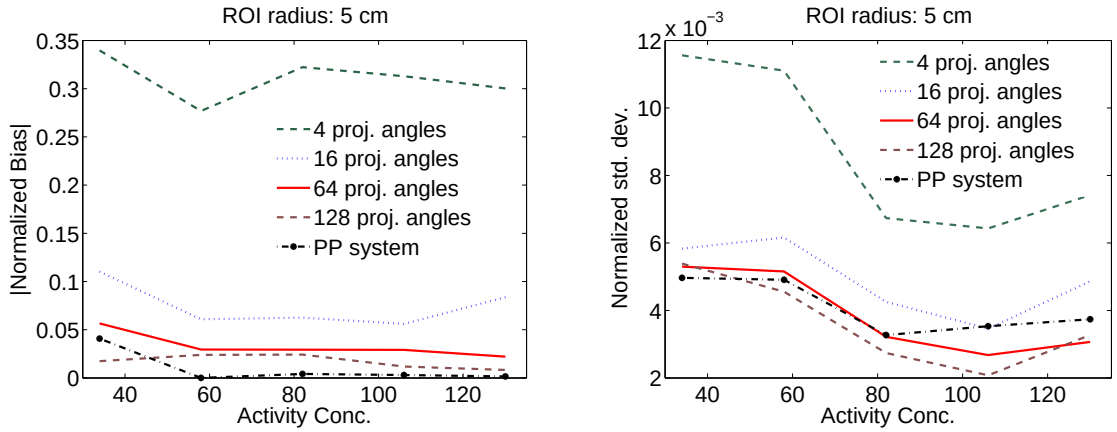

(a) (b)

Figure 5: (a) Normalized bias and (b) standard deviation of estimated activity as the number of projection angles is varied.

In general, the standard deviation of the estimated activities decreased with increasing activity and ROI size, but the variation was not smooth. This may be partially attributed to the fact that these are low-count experiments, and thus the noise effects could be dominant. We also observe from the results that the bias and standard deviation values were not very high for the PP systems, thus pointing to the efficacy of the proposed technique.

5. CONCLUSIONS AND FUTURE WORK

PC systems have infinite-dimensional null spaces due to dimensionality considerations. PP systems do not necessarily suffer from this issue. Based on this premise, we theoretically argued that PP systems could provide better performance at estimating the mean activity concentration in an ROI as compared to PC systems for various ROI templates and object functions. Further, we derived an SVD-based technique to estimate the activity concentration using PP systems. We then compared the performance of PP and PC systems in terms of estimating the mean activity concentration as a function of the ROI size, true activity concentration, and number of projection angles for PC systems. We observed that, in most cases, the PP system offered improved estimation performance measured in terms of bias and standard deviation of the estimated activity concentration values.

We are currently designing more optimal estimation techniques, in particular, a ML method, to estimate the mean activity concentration within the ROI. The ML method will help reduce estimation-related errors, so that we can compare the PP and PC systems more accurately on the task of estimating the mean activity concentration. Additionally, the ML method will also acccount for the estimation-related blur more accurately. Further, we are also studying the task of estimating the activity in phantoms consisting of multiple known ROIs.

Acknowledgments

This work was supported by National Institute of Biomedical Imaging and Bioengineering of the National Institutes of Health under grant numbers R01-EB000803, P41-EB002035, R01-EB016231 and EB013558. The authors would like to thank Dr. Harrison H. Barrett, Dr. Matthew Kupinski, and Dr. Eric Clarkson for helpful discussions.

REFERENCES

[1] Peterson, T. E. and Furenlid, L. R., "SPECT detectors: the Anger Camera and beyond," *Phys. Med. Biol.* **56**, R145–182 (Sep 2011).

[2] Barrett, H. H. and Myers, K. J., [*Foundations of Image Science*], Wiley (2004).

[3] Taguchi, K. and Iwanczyk, J. S., "Vision 20/20: Single photon counting X-ray detectors in medical imaging," *Med. Phys.* **40**, 100901 (Oct 2013).

[4] Jha, A. K., Kupinski, M. A., Masumura, T., Clarkson, E., Maslov, A. A., and Barrett, H. H., "Simulating photon-transport in uniform media using the radiative transfer equation: A study using the Neumann-series approach," *J. Opt. Soc. Amer. A.* **29**(8), 1741–1757 (2012).

[5] Barrett, H. H., Myers, K. J., Hoeschen, C., Kupinski, M. A., and Little, M. P., "Task-based measures of image quality and their relation to radiation dose and patient risk," *Phys. Med. Biol.* **60**(2), R1 (2015).

[6] [*Radiance and photon noise: imaging in geometrical optics, physical optics, quantum optics, and radiology*], **9193** (2014).

[7] Anger, H. O., "Scintillation camera," *Rev. Sci. Instrum.* **29**, 27–33 (1958).

[8] Barrett, H. H., Hunter, W. C., Miller, B. W., Moore, S. K., Chen, Y., and Furenlid, L. R., "Maximum-likelihood methods for processing signals from gamma-ray detectors," *IEEE Trans. Nucl. Sci.* **56**, 725 (Jun 2009).

[9] Hesterman, J. Y., Caucci, L., Kupinski, M. A., Barrett, H. H., and Furenlid, L. R., "Maximum-likelihood estimation with a contracting-grid search algorithm," *IEEE Trans. Nucl. Sci.* **57**, 1077–84 (Jun 2010).

[10] Caucci, L., Hunter, W. C., Furenlid, L. R., and Barrett, H. H., "List-mode MLEM image reconstruction from 3D ML position estimates," *IEEE Nucl Sci Symp Conf Rec* , 2643–2647 (2010).

[11] Jha, A. K., Barrett, H. H., Frey, E., Clarkson, E., Caucci, L., and Kupinski, M. A., "Singular value decomposition for photon-processing nuclear imaging systems and applications for reconstruction and computing null functions," *Phys. Med. Biol.* (in review).

[12] Furenlid, L. R., Wilson, D. W., Chen, Y. C., Kim, H., Pietraski, P. J., Crawford, M. J., and Barrett, H. H., "FastSPECT II: A second-generation high-resolution dynamic SPECT imager," *IEEE Trans. Nucl. Sci.* **51**, 631–635 (Jun 2004).

[13] Miller, B. W., Gregory, S. J., Fuller, E. S., Barrett, H. H., Barber, H. B., and Furenlid, L. R., "The iQID camera: An ionizing-radiation quantum imaging detector," *Nucl. Inst. Meth. in Phys. Res. Sec. A* **767**(0), 146 – 152 (2014).

[14] Miller, B. W., Barrett, H. H., Furenlid, L. R., Barber, H. B., and Hunter, R. J., "Recent advances in BazookaSPECT: Real-time data processing and the development of a gamma-ray microscope," *Nucl. Instrum. Meth. Phys. Res. A* **591**, 272–275 (Jun 2008).

[15] Marks, D., Barber, H., Barrett, H., Tueller, J., and Woolfenden, J., "Improving performance of a CdZnTe imaging array by mapping the detector with gamma rays," *Nucl. Inst. Meth. Phys. Res. Sec. A* **428**(1), 102 – 112 (1999).

[16] H. H. Barrett, H. B. Barber, J. E. and Marks, D., "Signal-processing method for gamma-ray semiconductor sensor," (Oct 1998).

[17] Moore, S., Barrett, H., and Furenlid, L., "ModPET - A compact PET system employing modular gamma cameras, maximum-likelihood event-parameter estimation, and list-mode ML-EM reconstruction," *J. Nucl. Med. Meeting Abstracts* **53**, 491 (2012).

[18] Jha, A. K., Clarkson, E., Kupinski, M. A., and Barrett, H. H., "Joint reconstruction of activity and attenuation map using LM SPECT emission data," in [*Proc. SPIE Med. Imag.*], **8668**, 86681W1–9 (2013).

[19] Dewaraja, Y. K., Frey, E. C., Sgouros, G., Brill, A. B., Roberson, P., Zanzonico, P. B., and Ljungberg, M., "MIRD pamphlet No. 23: Quantitative SPECT for patient-specific 3-dimensional dosimetry in internal radionuclide therapy," *J. Nucl. Med.* **53**, 1310–1325 (Aug 2012).

[20] Dewaraja, Y. K., Ljungberg, M., Green, A. J., Zanzonico, P. B., Frey, E. C., Bolch, W. E., Brill, A. B., Dunphy, M., Fisher, D. R., Howell, R. W., Meredith, R. F., Sgouros, G., and Wessels, B. W., "MIRD pamphlet No. 24: Guidelines for quantitative 131I SPECT in dosimetry applications," *J. Nucl. Med.* **54**, 2182–2188 (Dec 2013).

[21] Ljungberg, M., Sjogreen, K., Liu, X., Frey, E., Dewaraja, Y., and Strand, S. E., "A 3-dimensional absorbed dose calculation method based on quantitative SPECT for radionuclide therapy: evaluation for (131)I using Monte carlo simulation," *J. Nucl. Med.* **43**, 1101–1109 (Aug 2002).

[22] Zaidi, H. and Fakhri, G. E., "Is absolute quantification of dopaminergic neurotransmission studies with 123I SPECT ready for clinical use?," *Eur. J. Nucl. Med. Mol. Imag.* **35**, 1330–1333 (Jul 2008).

[23] Morton, R. J., Guy, M. J., Clauss, R., Hinton, P. J., Marshall, C. A., and Clarke, E. A., "Comparison of different methods of DatSCAN quantification," *Nucl. Med. Commun.* **26**, 1139–1146 (Dec 2005).

[24] Cao, X., Zurakowski, D., Diamond, D. A., and Treves, S. T., "Automatic measurement of renal volume in children using 99mTc dimercaptosuccinic acid SPECT: normal ranges with body weight," *Clin. Nucl. Med.* **37**, 356–361 (Apr 2012).

[25] Yen, T. C., Chen, W. P., Chang, S. L., Liu, R. S., Yeh, S. H., and Lin, C. Y., "Technetium-99m-DMSA renal SPECT in diagnosing and monitoring pediatric acute pyelonephritis," *J. Nucl. Med.* **37**, 1349–1353 (Aug 1996).

[26] Barrett, H. H., Aarsvold, J. N., and Roney, T. J., "Null functions and eigenfunctions: tools for the analysis of imaging systems," *Prog. Clin. Biol. Res.* **363**, 211–226 (1991).

[27] Lehovich, A., *List mode SPECT Reconstruction using Empirical Likelihood*, PhD thesis, College of Optical Sciences, University of Arizona, Tucson, AZ, USA (2005).

[28] Caucci, L. and Barrett, H. H., "Objective assessment of image quality. V. Photon-counting detectors and list-mode data," *J. Opt. Soc. Am. A* **29**, 1003–1016 (Jun 2012).

[29] Jha, A. K., Barrett, H. H., Clarkson, E., Caucci, L., and Kupinski, M. A., "Analytic methods for list-mode reconstruction," in [*Intl Meet Fully Three-Dim Image Recon Rad Nucl Med, California*], (2013).

[30] Huesman, R. H., "A new fast algorithm for the evaluation of regions of interest and statistical uncertainty in computed tomography," *Phys. Med. Biol.* **29**, 543–552 (May 1984).

[31] Ramachandran, G. N. and Lakshminarayanan, A. V., "Three-dimensional reconstruction from radiographs and electron micrographs: Application of convolutions instead of fourier transforms," *Proc. Natl. Acad. Sci. USA* **68**, 2236–40 (Sept. 1971).

[32] Papoulis, A. and Pillai, S. U., [*Probability, Random Variables and Stochastic Processes*], Tata McGraw-Hill, fourth ed. (2002).